

# Like-Charge Colloid-Polyelectrolyte Complexation

Rene Messina, Christian Holm,<sup>y</sup> and Kurt Kremer<sup>z</sup>

Max-Planck-Institut für Polymerforschung, Ackermannweg 10, 55128 Mainz, Germany

(Dated: April 14, 2024)

We investigate the complexation of a highly charged sphere with a long flexible polyelectrolyte, both negatively charged in salt free environment. Electroneutrality is insured by the presence of divalent counterions. Using molecular dynamics (MD) within the framework of the primitive model, we consider different Coulomb coupling regimes. At strong Coulomb coupling we find that the adsorbed chain is always connected to the colloidal surface but forms different conformations that depend on the linear charge density of the chain. A mechanism involving the polyelectrolyte overcharging is proposed to explain these structures. At intermediate Coulomb coupling, the chain conformation starts to become three-dimensional, and we observe multilayering of the highly charged chain while for lower charge density the chain wraps around the colloid. At weak Coulomb coupling, corresponding to an aqueous solvent, we still find like-charge complexation. In this latter case the chain conformation exhibits loops.

PACS numbers: 61.20.Qg, 82.70.Dd, 87.10.+e

## I. INTRODUCTION

The adsorption of polyelectrolytes onto an oppositely charged spherical particle has been experimentally extensively studied recently<sup>1,2,3,4</sup>. Various authors have investigated this phenomenon theoretically<sup>5,6,7,8,9,10,11,12,13</sup> and by Monte Carlo simulations<sup>14,15,16,17,18</sup>. Nonetheless, much less is known concerning the complexation of a charged sphere with a like-charged polyelectrolyte. It is only very recently that we reported in a short communication such a phenomenon in the strong Coulomb coupling regime<sup>19</sup>. From a theoretical point of view, the long range Coulomb interactions of these systems represents a formidable challenge, and especially the understanding of effective attraction of like charged bodies has attracted recent attention.

In this paper, we elaborate on the complexation between a sphere and a long flexible polyelectrolyte both negatively charged. While complexation in the strong coupling limit it is expected, we report new and rather unexpected chain conformations. We present MD simulation results without added salt but taking into account the counterions explicitly. Various Coulomb couplings as well as different polyelectrolyte linear charge densities are investigated. A detailed study of the ions (monomer and counterion) distribution is reported and mechanisms accounting for the different encountered complex structures are proposed.

The paper is organized as follows. Section II contains details of our MD simulation model. Section III is devoted to the strong Coulomb coupling regime. Section IV is devoted to the intermediate Coulomb coupling regime. In Sec. V, we consider the like-charge complexation in the weak Coulomb coupling regime corresponding to water solvent.

## II. SIMULATION METHOD

The MD method employed here is based on the Langevin equation and is similar to that employed in previous studies<sup>20</sup>. Consider within the framework of the primitive model one spherical macroion characterized by a diameter  $d$  and a bare charge  $Q_M = Z_M e$  (where  $e$  is the elementary charge and  $Z_M > 0$ ) surrounded by an implicit solvent of relative dielectric permittivity  $\epsilon_r$ . The polymer chain is made up of  $N_m$  monomers of diameter  $a$ . Both ends of the chain are always charged and each  $l$ -th monomer is charged so that the chain contains  $N_{cm} = (N_m - 1)f + 1$  charged monomers. The monomer charge is  $q_m = Z_m e$  (with  $Z_m > 0$ ). The  $s$ -th all counterions, assumed all identical, ensure global electroneutrality and have a diameter  $a_c$  and charge  $+Z_c e$  (with  $Z_c > 0$ ). All these particles making up the system are confined in an impermeable spherical cell of radius  $R$ , and the spherical macroion is held fixed at the center of the cell.

The equation of motion of any mobile particle (counterion or monomer)  $i$  reads

$$m \frac{d^2 \mathbf{r}_i}{dt^2} = -\nabla \mathbf{r}_i U(\mathbf{r}_i) - \gamma \frac{d\mathbf{r}_i}{dt} + \mathbf{W}_i(t); \quad (1)$$

where  $m$  is the mass particle (supposed identical for all mobile species),  $U$  is the total potential force and  $\gamma$  is the friction coefficient. Friction and stochastic force are linked by the dissipation-fluctuation theorem  $\langle \mathbf{W}_i(t) \mathbf{W}_j(t') \rangle = 6m \gamma k_B T \delta_{ij} \delta(t - t')$ .

Excluded volume interactions are introduced via a pure short range repulsive Lennard-Jones (LJ) potential given by

$$U_{LJ}(r) = \begin{cases} 4 \left( \frac{r_0}{r} \right)^{12} - \left( \frac{r_0}{r} \right)^6 + \epsilon_0; & \text{for } r \leq r_{cut}; \\ 0; & \text{for } r > r_{cut}; \end{cases} \quad (2)$$

where  $r_0 = 0$  for the macroion-macroion interaction,  $r_0 = 7$  for the macroion-microion interaction and  $r_{cut} = 2^{1/6}$  is the cutoff radius. This leads to  $d = 2r_0 + 1 = 15$ , whereas the closest center-center distance of the microions to the spherical macroion is  $a = r_0 + 1 = 8$ . The macroion volume fraction is defined as  $f_M = (a/R)^3$  and is fixed to  $8 \cdot 10^{-3}$  with  $R = 40$ .

The pairwise electrostatic interaction between any pair  $ij$ , where  $i$  and  $j$  denote either a macroion or a charged microion (counterion or charged monomer), reads

$$\frac{U_{coul}(r)}{k_B T} = l_B \frac{Z_i Z_j}{r}; \quad (3)$$

where  $l_B = e^2 / (4\pi\epsilon_0 k_B T)$  is the Bjerrum length. Energies are measured in units of  $\epsilon = k_B T$  with  $T = 298$  K. Choosing  $\epsilon = 3.57$  Å requires that the Bjerrum length of water at room temperature equals  $2.7$  (7.14 Å). In this work the macroion charge is fixed at  $Z_M = 180$ .

The polyelectrolyte chain connectivity is modeled by using a standard finitely extensible nonlinear elastic (FENE) potential in good solvent (see for example Ref.<sup>20</sup>), which reads

$$U_{FENE}(r) = \begin{cases} \frac{1}{2} R_0^2 \ln \left( 1 - \frac{r^2}{R_0^2} \right); & \text{for } r < R_0; \\ 1; & \text{for } r \geq R_0; \end{cases} \quad (4)$$

where  $k$  is the spring constant-like chosen as  $1000 k_B T = 2$  and  $R_0 = 1.5$ . These values lead to an equilibrium bond length  $l = 0.8$ .

Typical simulation parameters are summarized in Table I. The simulation runs are reported in Table II. Each simulation run requires about  $10^7$  MD steps, and equilibrium is typically reached after  $5 \cdot 10^6$  up to  $3 \cdot 10^6$  steps. We normally performed between  $5 \cdot 10^6$  and  $10^7$  MD steps to take measurements. We cover the whole range of strength of Coulomb electrostatic interaction from the strong coupling limit, which is more theoretical interest, to the weak coupling limit, which corresponds to an aqueous solvent.

TABLE I: General data of the simulation model. Note that the temperature is used as energy scale for the simulations.

parameters	
$\epsilon = 3.57$ Å	Lennard Jones length units
$T = 298$ K	room temperature
$\epsilon = k_B T$	Lennard Jones energy units
$Z_M = 180$	macroion valence
$Z_m$	monomer valence
$Z_c$	counterion valence
$N_c$	total number of counterions
$l_B$	Bjerrum length
$a = 8$	macroion-counterion distance of closest approach
$R = 40$	simulation cell radius
$f_M = 8 \cdot 10^{-3}$	macroion volume fraction
$\epsilon = 1000 k_B T = 2$	FENE spring constant
$R_0 = 1.5$	FENE cutoff
$l = 0.8$	average bond length
$N_m$	total number of monomers
$N_{cm}$	number of charged monomers
$f$	monomer charge fraction
$p_E = Z_m \epsilon f = 1$	polyelectrolyte linear charge density

TABLE II: Specification of the simulated systems. The chain radii of gyration  $R_g^{(\text{bulk})}$  and  $R_g^{(\text{comp})}$  are given for an isolated chain (i.e., in the absence of the colloid) and for the complexation case (i.e., in the presence of the colloid) respectively. Lengths are in units of  $\sigma$ .

parameter	$l=f$	$N_m$	$N_{cm}$	$N_c$	$Z_m$	$Z_c$	$l_b$	$R_g^{(\text{bulk})}$	$R_g^{(\text{comp})}$
run A	1	256	256	346	2	2	10	3.81	6.42
run B	2	257	129	219	2	2	10	3.90	8.69
run C	3	256	86	176	2	2	10	3.95	8.75
run D	5	256	52	142	2	2	10	4.49	8.86
run E	1	256	256	346	2	2	4	4.40	4.8
run F	2	257	129	219	2	2	4	4.8	9.4
run G	3	256	86	176	2	2	4	5.4	9.3
run H	1	256	256	346	2	2	2	6.6	6.1
run I	2	257	129	219	2	2	2	12	13
run J	3	256	86	176	2	2	2	–	21
run K	1	256	256	436	1	1	2	–	–

### III. STRONG COULOMB COUPLING

First we look at the like-charge complexation in the strong Coulomb coupling regime. We choose the relative permittivity  $\epsilon_r = 16$ , corresponding to  $l_b = 10$ , and divalent microions ( $Z_m = Z_c = 2$ ). Such a set of parameters is of special theoretical interest to study the influence of strong electrostatic correlations.

#### A. Single charged object

In this section we first study separately (i) the spherical macroion and (ii) the flexible polyelectrolyte in the presence of their surrounding neutralizing divalent counterions separately. This provides the reference states for the more complicated situation, where both of these two objects interact.

##### 1. Spherical macroion

Consider an isolated macroion with its surrounding divalent counterions. A pertinent parameter to describe the Coulomb coupling for such highly asymmetric electrolyte solution (macroion and counterions) is the so-called "plasma" parameter  $\Gamma = Z_c^2 l_b / a_{cc}$ , where  $a_{cc}$  (which will be determined below) is the average distance (triangular lattice parameter in the ground state) between counterions lying on the macroion surface<sup>21</sup>. For the strong Coulomb coupling considered we find  $\Gamma \approx 13$  (with  $l_b = 180$ ), and for finite macroion volume fraction (here  $\phi_i = 8 \cdot 10^{-3}$ ), all counterions lie in the vicinity of the macroion surface<sup>22,23,24,25</sup>.

To characterize the counterion layer structure, we compute the counterion correlation function  $g(s)$  on the surface of the sphere<sup>23,25</sup>, defined as:

$$c^2 g(s) = \frac{1}{N_c} \sum_{i \neq j}^* \frac{1}{|\mathbf{r}_i - \mathbf{r}_j|} \quad (5)$$

where  $c = N_c / 4\pi a^2$  is the surface counterion concentration ( $N_c = Z_m = Z_c$  being the number of counterions), and  $s = |\mathbf{r}_i - \mathbf{r}_j|$  corresponds to the arc length on the sphere of radius  $a$  (center-distance of closest approach of macroion and counterion). Each counterion (located in the vicinity of the surface) is radially projected on the ("contact") shell around the macroion center of radius  $a = 8 \cdot \sigma$ . Correlation functions are computed by averaging  $g(s)$  over 1000 independent equilibrium configurations which are statistically uncorrelated. The pair distribution  $g(s)$  is normalized as follows

$$\int_0^{2\pi a} g(s) ds = (N_c - 1) \quad (6)$$

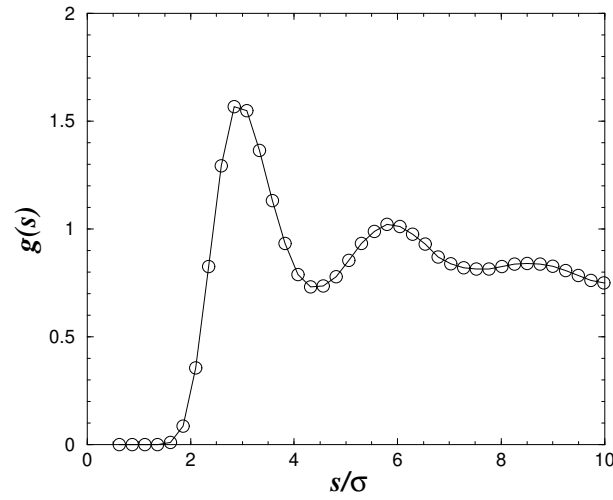


FIG. 1: Counterion surface correlation function  $g(s)$  for the 90 divalent counterions ( $Z_M = 180$ ) in the case of an isolated macroion in strong Coulomb coupling ( $\ell_b = 10$ ). See Fig. 2 for a typical equilibrium snapshot.



FIG. 2: Snapshot of the equilibrium counterion structure of an isolated macroion with a bare charge  $Z_M = 180$  [see Fig. 1 for the corresponding  $g(s)$ ].

Because of the finite size and the topology of the sphere,  $g(s)$  has a cut-off at  $a$  ( $\approx 25.1$ ) and a zero value there. Therefore, at large values of  $s$ ,  $g(s)$  cannot directly be compared to the correlation function in an infinite plane.

Results are depicted in Fig. 1 for  $Z_M = 180$ . The first peak<sup>1</sup> appears at about  $s = a_{cc} \approx 3$  whereas the second peak about  $s \approx 6$  and finally the third small peak around  $s \approx 9$ . This structure, which is highly correlated, is referred to as a strongly correlated liquid (SCL)<sup>23,26</sup>, but not yet a Wigner crystal. A typical equilibrium configuration is depicted in Fig. 2 where one can see the local arrangement close to a triangular lattice.

---

<sup>1</sup> It is this value  $a_{cc} \approx 3$  which gives  $\rho \approx 13$ .

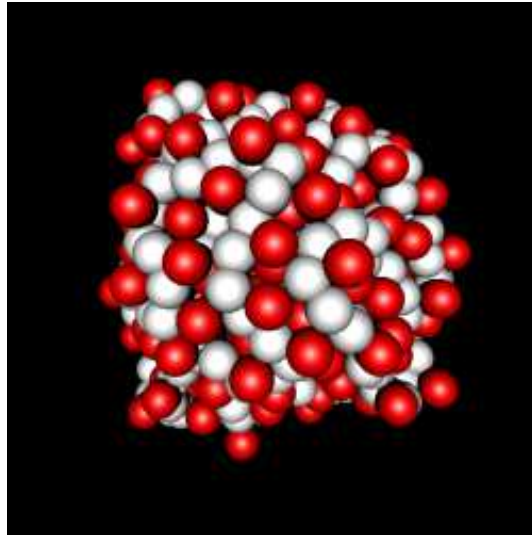


FIG. 3: Snapshot of the equilibrium conformation of an isolated polyelectrolyte chain made up of 256 monomers where all monomers are charged ( $f = 1$ ). Monomers are in white and counterions in dark grey.

## 2. Polyelectrolyte chain

Now we investigate an isolated polyelectrolyte chain together with its surrounding divalent counterions in bulk confined to the same spherical cell of radius  $R = 40$ . We consider four monomer charge fractions (i. e. four linear charge densities)  $f = 1, 1/2, 1/3$  and  $1/5$ . The chain is made up of  $N_m = 256$  monomers ( $N_m = 257$  for  $f = 1/2$ ). while  $Z_m = Z_c = 2$ , The polymer chain parameters are identical to those of the complexation case (see Table II). The chain extension is characterized by its radius of gyration  $R_g$  given by

$$R_g^2 = \frac{1}{N_m} \sum_{i=1}^{N_m} (\mathbf{r}_i - \mathbf{r}_{CM})^2; \quad (7)$$

where  $\mathbf{r}_{CM}$  is the center of mass position of the chain.

The corresponding values of  $R_g$  can be found in Table II (see  $R_g^{(bulk)}$  for runs A-D). The chain extension varies little with  $f$  and is roughly given by  $R_g \approx 4$ . For this strong Coulomb coupling, all counterions are "condensed" into the polyelectrolyte globule for all three linear charge densities considered. The strong counterion condensation induces a collapse of the chain, which is by now well understood<sup>27,28,29,30,31</sup>. A typical equilibrium chain conformation is shown in Fig. 3 for  $f = 1$ . As expected the structure is very compact and highly ordered. Very similar structures are obtained for  $f = 1/2, 1/3$  and  $1/5$ .

## B. Complexation

We now investigate the complexation of a highly charged colloid with a long flexible polyelectrolyte, both negatively charged. Four different parameter combinations, denoted by run A, B, C and D, were investigated which are summarized in Table II. Going from run A to D the polyelectrolyte charge fraction  $f$  decreases from 1 to  $1/5$ . The contour length of the chain is much larger ( $N_m \approx 14$  times) than the colloidal particle diameter.

### 1. Observation of the complexation

Figure 4 shows typical equilibrium configurations of the colloid-polyelectrolyte complex. We notice that in all reported cases complexation occurs and the polyelectrolyte is completely adsorbed onto the colloidal surface, that is, in presence of a highly charged colloid, the polyelectrolyte conformation becomes quasi two-dimensional in contrast to the bulk case (compare Fig. 4 with Fig. 3). However the structure of these resulting complexes depends strongly on

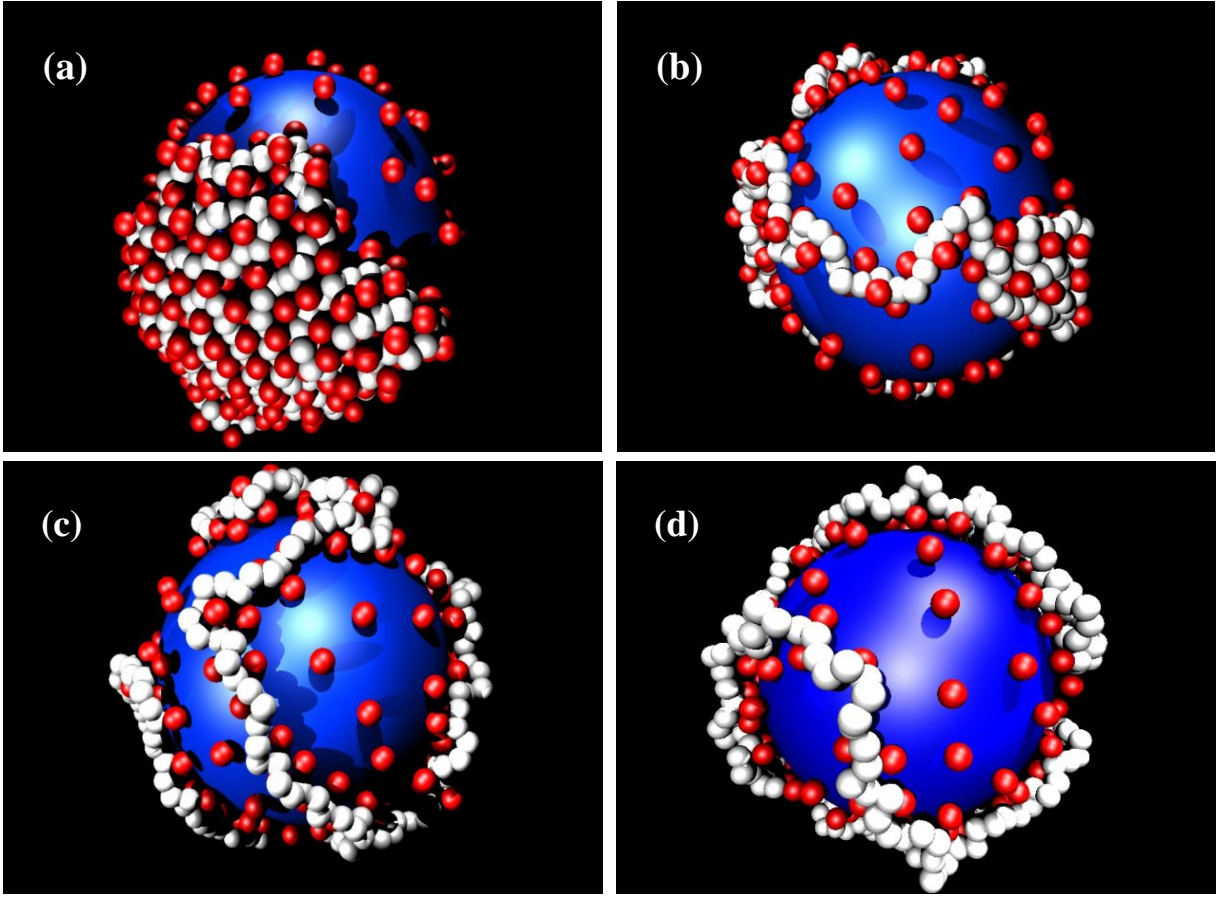


FIG. 4: Typical equilibrium configurations of the colloid-polyelectrolyte complex in strong Coulomb coupling ( $l_b = 10$ ) for (a) run A ( $f = 1$ ), (b) run B ( $f = 1/2$ ), (c) run C ( $f = 1/3$ ) and (d) run D ( $f = 1/5$ ). Monomers are in white and counterions in red.

the value of  $f$ . For the fully charged polyelectrolyte case [run A with  $f = 1$  – see Fig. 4 (a)] the monomers are closely packed forming a two-dimensional compact Hamiltonian-walk with the condensed counterions on the polyelectrolyte. This structure consists of closed packed lines made from either counterions or monomers. When the linear charge density is reduced [see Fig. 4 (b-d)], the complex structures are qualitatively different. In these cases the monomers are no longer closely packed. For run B [ $f = 1/2$ , Fig. 4 (b)], the monomers spread more over the particle surface and the polymer partially wraps around the sphere exhibiting a quasi two-dimensional surface pearl-necklace structure. For run C [ $f = 1/3$ , Fig. 4 (c)] and run D [ $f = 1/5$ , Fig. 4 (d)], the monomers spread entirely over the particle surface, and the chain wraps the colloidal particle leading to an almost isotropic distribution of the monomers around the spherical macroion.

The like-charge complex formation is due to the strong counterion mediated correlations which are known to induce attractions in the strong Coulomb coupling regime. Basically, the charged species will try to order locally in a way which is compatible with the chain connectivity and the macroion surface constraints. We now quantify those observations and propose a simple mechanism to explain the observed conformations.

## 2. Adsorption profile

To quantify the adsorption of the monomers and counterions on the macroion particle surface, we analyze three quantities: (i) the ion radial distribution function  $n_i(r)$ , (ii) the ion fraction  $P_i(r)$  and (iii) the net fluid charge  $Q_i(r)$  (omitting the macroion bare charge  $Z_M$ ), where  $r$  is the distance from the spherical macroion center. The radial ion distribution function  $n_i(r)$  is normalized as follows

$$\int_{r_0}^{R_r} n_i(r) 4\pi r^2 dr = N_i \text{ with } i = c; m; \quad (8)$$

where  $N_i$  is the total number of ions, and the subscripts  $c$  and  $m$  stand for counterion and monomer respectively. The reduced integrated ion radial density  $P_i(r)$  is linked to  $n_i(r)$  via

$$P_i(r) = \frac{\int_{r_0}^R n_i(r') 4\pi r'^2 dr'}{N_i} \text{ with } i = c; m; \quad (9)$$

Note that for  $f < 1$ , neutral and charged monomers are all included in the quantities  $n_m(r)$  and  $P_m(r)$ . The net fluid charge  $Q(r)$  is given by

$$Q(r) = \int_{r_0}^R [Z_c n_c(r') - Z_m n_m(r')] 4\pi r'^2 dr'; \quad (10)$$

where we choose  $e = 1$ .

Integrated distribution  $P(r)$ , radial distribution  $n(r)$  and fluid net charge  $Q(r)$  profiles are depicted in Figs. 5(a-c) respectively. Fig. 5(a) shows that all atoms for all runs are condensed within a distance of about 10 from the colloid

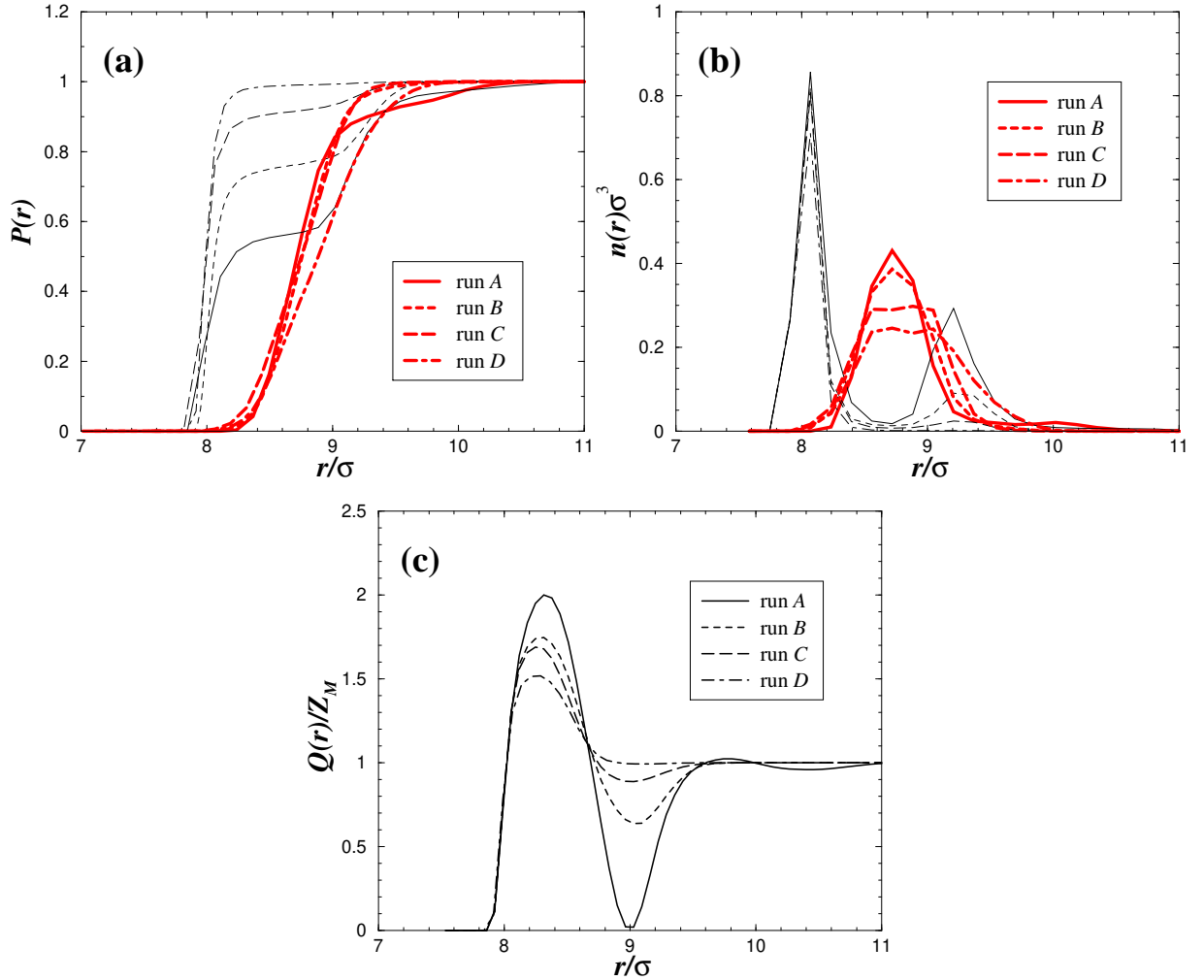


FIG. 5: Ion adsorption profiles (runs A – D) as a function of the distance  $r$  from the macroion center. (a) Fraction  $P(r)$  and (b) radial density  $n(r)$  of counterions (thin lines) and monomers (thick lines) – (c) reduced net fluid charge  $Q(r) = Z_M$ .

center and more than 80% of the monomers and counterions are within a distance of  $9.3\sigma$  from the colloid center corresponding roughly to two atomic layers [see also the radial distribution in Fig 5(b)]. Due to strong electrostatic attraction between the sphere and the counterions and strong electrostatic repulsion between the sphere and the charged monomers the first layer ( $r = a = 8\sigma$ ) is exclusively made up of counterions [see Figs 5(a-b)]. Note that the monomer depletion in this first counterion layer also concerns neutral monomers (runs B-D) and this effect is attributed to the chain connectivity. This means that the repulsion stemming from the charged monomers impose the polymer structure as long as  $f$  and the Coulomb coupling are sufficiently high, which is the case in the present study. The height of the first peak in the counterion  $n_c(r)$  profile is almost independent on  $f$ . The second ion layer is mixed of monomers and counterions, however with a majority of monomers [see Figs 5(a-b)]. Indeed the first monomer peak in the  $n_m(r)$  profile (located at  $r = 8.7\sigma$ ) and the second counterion peak in the  $n_c(r)$  profile (located at  $r = 9.2\sigma$ ) are only separated by roughly  $r = 0.5\sigma$  [see Fig 5(b)]. This leads to a medium position located at  $r = 9\sigma$  corresponding to a bilayer thickness. The height of the second peak in the counterion  $n_c(r)$  profile increases with increasing  $f$  [see Fig 5(b)].

For  $f = 1$  (run A), we observe a massive macroion charge inversion of more than 100% [i.e.  $Q(r) = Z_M > 2$ ] in the first layer as well as a strong charge oscillation [see Fig. 5(c)]. Upon reducing  $f$  (runs B-D) the macroion charge overcompensation decreases as well as the charge oscillation amplitude [see Fig. 5(c)]. This is due to the fact that upon reducing  $f$  less counterions are present and their correlations change.

### 3. Polyelectrolyte chain radius of gyration

Next, we investigate the radius of gyration  $R_g$  of the chain, i.e. Eq. (7), in order to gain insight of the spreading of the monomers over the sphere. The results reported in Fig. 6 (for  $l_b = 10\sigma$ ) show that  $R_g$  increases with decreasing  $f$  which demonstrates that the spreading of the monomers over the macroion surface is enhanced by decreasing the polyelectrolyte charge density. The jump in  $R_g$  is particularly large between  $f = 1$  and  $f < 1$ . This is in agreement with the visual inspection of the chain conformations presented in Fig. 4. Moreover, the isotropic case (monomers fully spread over the particle) corresponding to  $R_g = 8.7\sigma$ <sup>2</sup> is already reached for  $f = 1/2$  (run B).

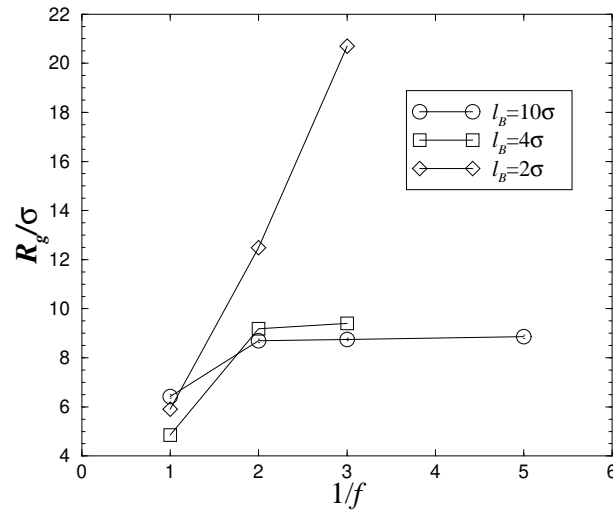


FIG. 6: Radius of gyration of the polymer as a function of the polyelectrolyte charge fraction  $f$  for  $l_b = 10\sigma$  (runs A-D),  $l_b = 4\sigma$  (runs E-F) and  $l_b = 2\sigma$  (runs G-H).

<sup>2</sup> This value corresponds to the first monomer peak position in the  $n_m(r)$  profile [see Fig 5(b)].



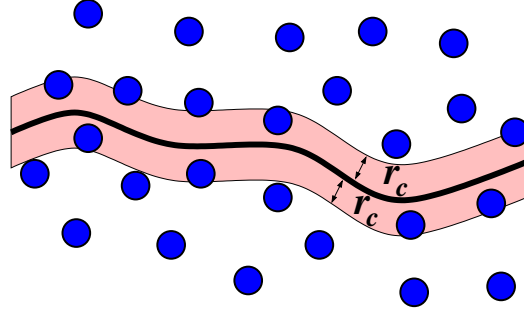


FIG. 7: Schematic view of the chain intercepting counterions within a distance  $r_c$ .

#### 4. Surface counterion correlation function

In this section we are interested in determining the structure of the "free" counterions which are not condensed onto the polyelectrolyte chain. Counterions are called "condensed" on the polyelectrolyte chain when they lie within a distance  $r_c = 1.2$  perpendicular to the chain (Fig. 7). All other counterions are called "free", although they are still adsorbed onto the colloidal surface. To characterize the structure of the free counterions we proceed in the same way as in Sec. III A 1. The surface free counterion correlation function  $g_{free}(s)$  is now given by

$$c_{free}^2 g_{free}(s) = \frac{1}{N_{free}^2} \sum_{i \neq j}^* \langle s_i^0 s_j^0 \rangle \quad (11)$$

where the sum in Eq. (11) is restricted to the free counterions, and  $c_{free} = N_{free}/a^2$  is the surface free counterion concentration, with  $N_{free}$  being the average number of free counterions. The normalization is obtained as follows

$$c_{free} \int_0^\infty g_{free}(s) ds = (N_{free} - 1) \quad (12)$$

Results are depicted in Fig. 8 for runs A-D. The important result is that the first peak of  $g_{free}(r)$  is located at the same position ( $s \approx 3$ ) as in the "unperturbed" case of an isolated macroion (without polyelectrolyte) studied in Sec. III A 1 (see Fig. 1). Although the second peak of  $g_{free}(s)$  is less pronounced than in the "unperturbed" case (compare Fig. 8 with Fig. 1), the local order of the free counterion structure is still high as can be visually inspected

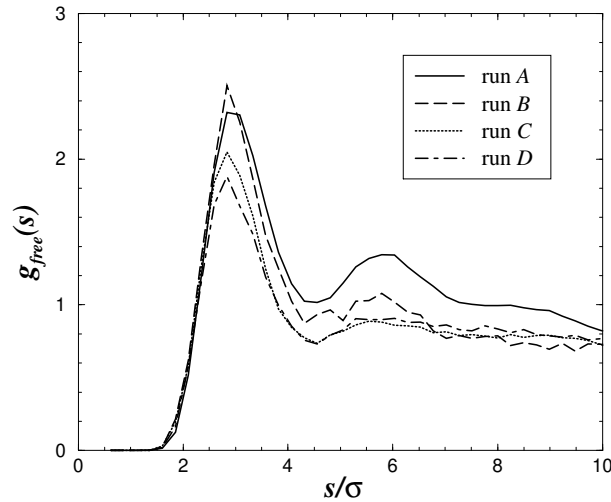


FIG. 8: Free counterion (unbound to the polyelectrolyte) surface correlation function  $g_{free}(s)$  for runs A-D.

on the snapshots sketched in Fig. 4. Thus the adsorbed chain only affects the counterion distribution significantly in its immediate neighborhood.

### 5. Polyelectrolyte overcharging

We now show that the concept of polyelectrolyte overcharging can be used to explain the observed complex structures. Let  $N_{cd}$  be the number of counterions we consider as condensed onto the polyelectrolyte. Then the overcharging ratio  $\chi_{PE}$  is defined as

$$\chi_{PE} = \frac{N_{cd}}{N_{cm}}; \quad (13)$$

which is merely the ratio between the amount of the total condensed counterion charge and the polyelectrolyte bare charge.

This "overcharging" can also be analytically predicted by the simple assumption that the presence of the polyelectrolyte (with its counterions) does not affect the free counterion distribution<sup>3</sup>. Let us consider the bare charged chain plus its own neutralizing counterions as an uncharged object that gets overcharged by intercepting all counterions (of the macroion) whose center lie within a ribbon of width  $2r_c$  and area  $A_{rib} = 2r_c N_m l$  (Fig. 7). If  $c$  is the counterion (of the macroion) concentration then the theoretical overcharging ratio  $\chi_{th}$  is merely given by

$$\chi_{th} = 1 + \frac{A_{rib}C}{N_{cm}} = 1 + \frac{2r_c N_m l Z_M}{N_{cm} Z_c 4 a^2}; \quad (14)$$

and since the number of charged monomers  $N_{cm}$  is given by  $N_{cm} = (N_m - 1)f + 1$ , Eq. (14) reduces for  $N_m \gg 1$  to

$$\chi_{th} = 1 + C = f; \quad (15)$$

with  $C = \frac{2r_c l Z_M}{Z_c 4 a^2}$ .

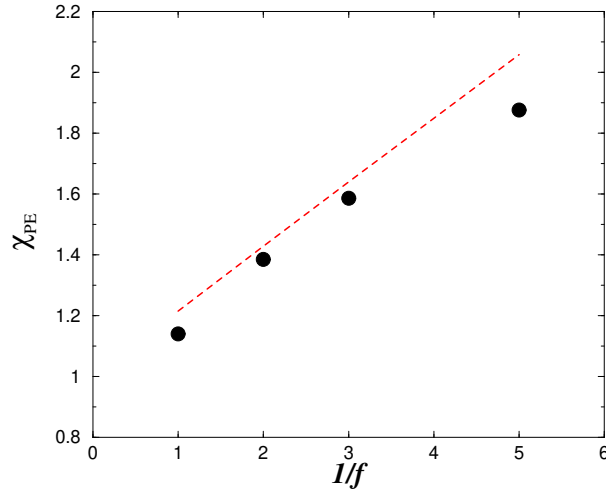


FIG. 9: Polyelectrolyte overcharge as a function of  $f$  (runs A-D). The dashed line corresponds to the theoretical prediction where Eq. (14) was used.

<sup>3</sup> This mainly holds for the first correlational peak which is the most important for the present discussion, as we showed in the previous Sec. IIIB 4.

TABLE III: Polyelectrolyte overcharge  $\rho_{PE}$  values as a function of  $f$ .

Run	$1=f$	$\rho_{PE}$ - MD	$\rho_{PE}$ - Theory
A	1	1.140 0.002	1.21
B	2	1.39 0.02	1.43
C	3	1.59 0.02	1.64
D	5	1.88 0.03	2.06

Results are presented in Fig. 9 and the corresponding values can be found in Table III. It indicates that in all cases overcharging occurs (i.e.,  $\rho_{PE} > 1$ ), and that it increases with decreasing polyelectrolyte charge density. We have excellent agreement (less than 10% difference) between simulation results and our toy model [Eq. (14)]. In turn it explains why  $\rho_{PE}$  varies almost linearly with  $1=f$  in our simulations.

The  $f$ -dependency of the complexation structure can be explained through the overcharging. For this we consider the overcharged polyelectrolyte as a dressed (or renormalized) chain [bare chain + counterions] with an (or renormalized) linear charge density  $\rho_{PE} = (\rho_{PE} - 1) \rho_{PE}$  that obviously has the opposite sign of  $\rho_{PE}$ <sup>32</sup>. Similarly one can define the renormalized charge of a monomer as

$$q_m = (\rho_{PE} - 1) q : \quad (16)$$

Using Eq. (16) and the results of Fig. 9 this shows that  $q_m$  increases with increasing  $1=f$ . The overcharging leads to an effective local repulsion of the monomers, and subsequently to a bond stiffening of the chain. This in turn explains why the chain expands with increasing  $1=f$  (see Fig. 6 and Fig. 4 for the corresponding structures)<sup>33</sup>.

#### IV. INTERMEDIATE COULOMB COUPLING

In this section we are dealing with a higher dielectric constant ( $\epsilon_r = 40$ ), meaning that we consider weaker Coulomb coupling ( $l_b = 4$ ). Experimentally this could correspond to using alcohol as a solvent. We consider a set of three runs E - G with  $l_b = 4$  (see Table II). Thus these systems are, up to a shorter Bjerrum length  $l_b$ , identical to runs A - C. It will be helpful to start the discussion with the description of the observed complex microstructures.

##### A. Complex microstructure

Typical equilibrium macroion-polyelectrolyte complex structures are sketched in Fig. 10. When the polyelectrolyte is fully charged ( $f = 1$ , run E), Fig. 10(a) shows again a strongly compact chain conformation. But in the present situation the chain does not spread on the macroion surface as it was the case in the strong Coulomb coupling [compare Fig. 10(a) with Fig. 4(a)]. In fact the conformation of the charged chain in presence of the macroion is very similar to the bulk conformation [compare 10(a) with Fig. 3].

By reducing the monomer charge fraction, Figs. 10(b-c) show that the complex microstructure for runs F/G is again qualitatively different from the fully charged case (run E). For these smaller polyelectrolyte linear charge densities ( $f = 1/2$  and  $f = 1/3$ ), the chain conformation is again almost wrapping around the colloid. For  $f = 1/2$  (run F) the pearl-necklace structure observed in the strong Coulomb coupling [see Fig. 4(b)] does not appear here, instead small loops appear [see Fig. 10(b)]. For the smallest monomer charge fraction ( $f = 1/3$ , run G) the monomers fully spread over the macroion surface and the conformation is not compact, and also small loops appear [see Fig. 10(c)]. Again it is observed that upon reducing the polymer charge density the chain expands, but this time it expands also into the radial direction away from the macroion.

The forthcoming sections are devoted to study in more detail the monomer and counterion distributions.

##### B. Adsorption profile

Integrated distribution  $P(r)$ , radial distribution  $n(r)$  and fluid net charge  $Q(r)$  profiles are given in Figs. 11(a-c) respectively. In a general manner, the fraction of monomers and counterions in the vicinity of the macroion surface is clearly smaller than the one obtained in the strong Coulomb coupling as expected [compare Fig. 11(a) with Fig. 5(a)]. Also the width in  $P(r)$  profile of adsorbed ions is enlarged with decreasing Coulomb coupling [compare Fig. 11(a) with Fig. 5(a)]. These features show that the monomer adsorption is more diffuse (in the normal direction to

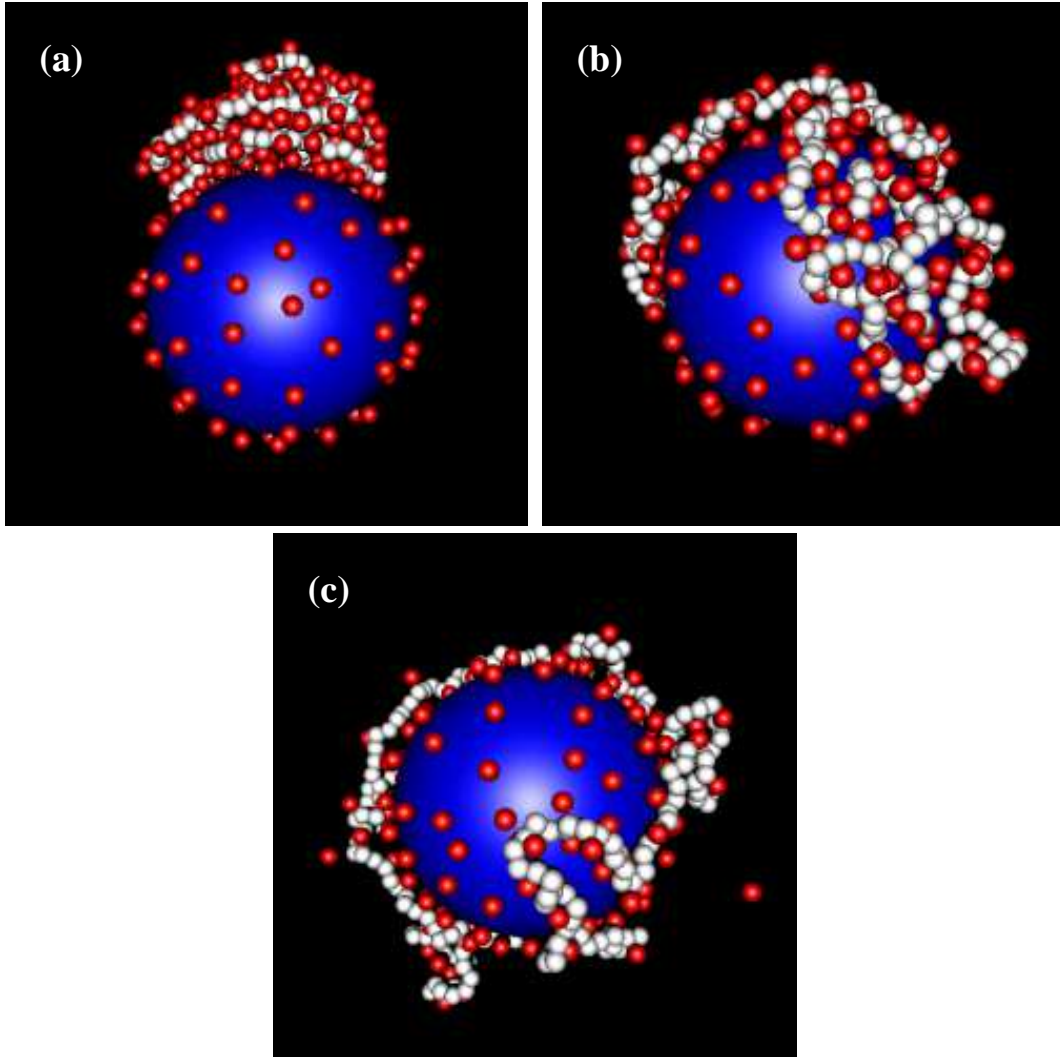


FIG. 10: Typical equilibrium configurations of the colloid-polyelectrolyte complex in moderate Coulomb coupling ( $l_B = 4$ ) for (a) run E ( $f = 1$ ), (b) run F ( $f = 1/2$ ) and (c) run G ( $f = 1/3$ ). Monomers are in white and counterions in red.

the macroion sphere) as expected for a weaker Coulomb coupling. Concerning the ion density  $n(r)$  profile [see Fig. 11 (b)], it is interesting to note that the height of the first peak in the monomer density  $n_m(r)$  profile is twice smaller for  $f = 1$  than for  $f < 1$ , whereas the one from the counterion density profile is almost independent on  $f$ . In parallel, the macroion charge overcompensation as well as charge oscillation amplitudes are clearly reduced compared to the strong Coulomb regime [compare Fig. 11 (c) with Fig. 5 (c)].

For the fully charged polyelectrolyte case ( $f = 1$ , run E) the  $n_m(r)$  profile in Fig. 11 (b) shows a strong second monomer peak and a weaker third one in agreement with the snapshot of Fig. 10 (a). The radial monomer ordering naturally goes along with a counterion ordering in antiphase. In other words, multilayering of different chain segments occurs, but without strong adsorption of the macroion [compare Fig. 10 (a) with Fig. 4 (a)]. Therefore we find three charge oscillations [see Fig. 11 (c)] against only two in the strong Coulomb coupling [see Fig. 5 (c)].

For smaller linear charge density, Fig. 11 (a) and Fig. 11 (b) indicate that for runs F ( $f = 1/2$ ) and G ( $f = 1/3$ ) the chain is almost fully adsorbed to the macroion surface without monomer chain multilayering [i. e., no appearance of monomer second peak in the  $n_m(r)$  profile – see Fig. 11 (b)]. However, the conformation is a little bit swollen probably due to the onset of loop formation, compare the snapshots in Fig. 10. As in the strong Coulomb coupling case, we find here only one charge oscillation for  $f = 1/2$  and  $f = 1/3$ , and the amplitude of the reduced net fluid charge decreases with decreasing  $f$ .

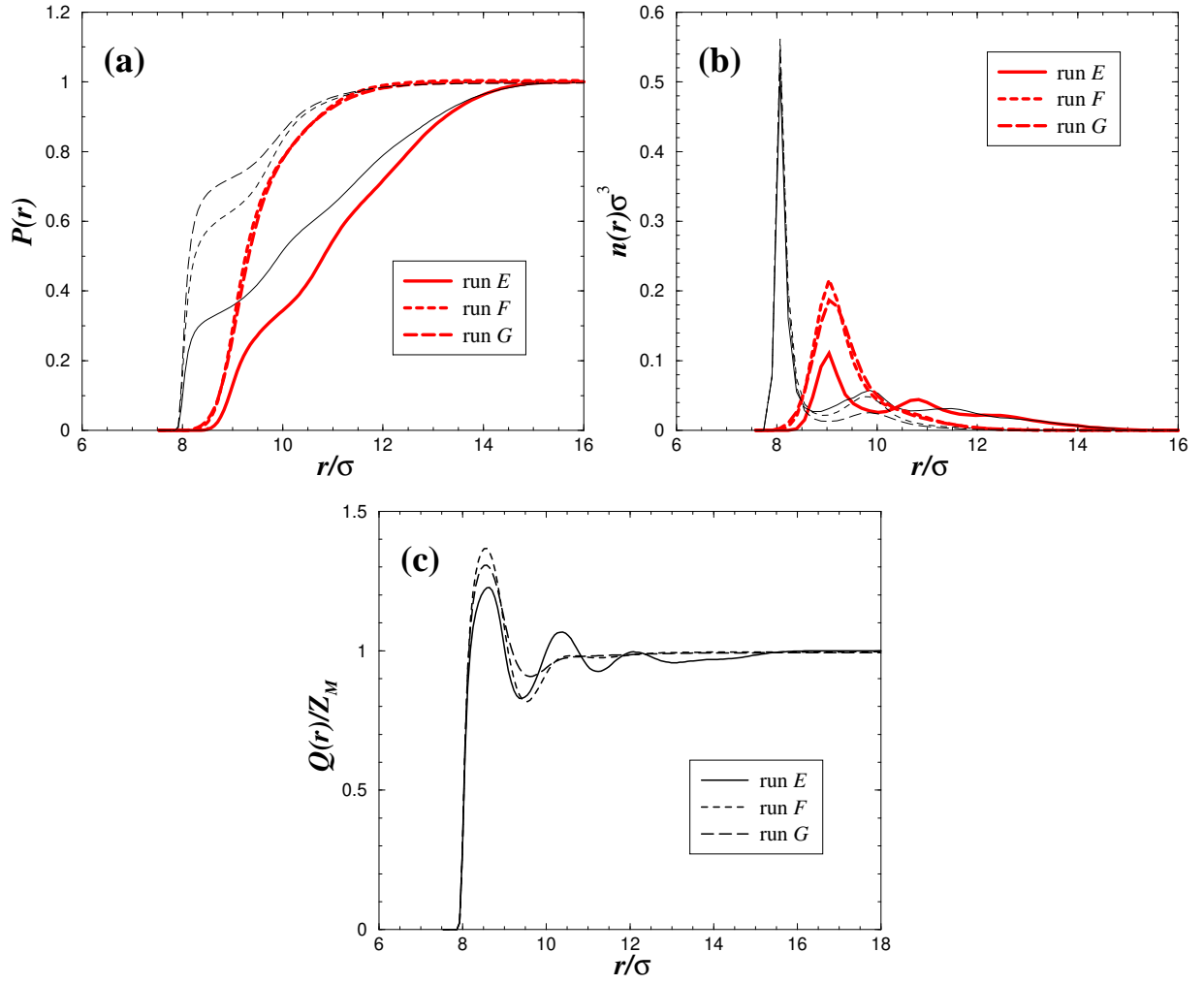


FIG. 11: Ion adsorption profiles (runs E – G) as a function of the distance  $r$  from the macroion center. (a) Fraction  $P(r)$  and (b) radial density  $n(r)$  of counterions (thin lines) and monomers (thick lines) – (c) reduced net fluid charge  $Q(r)/Z_M$ .

### C. Polyelectrolyte chain radius of gyration

Results for the radius of gyration  $R_g$  of the polymer chain are reported in Fig. 6 (for  $l_b = 4$ ). As for the high Coulomb coupling case with  $l_b = 10$ ,  $R_g$  increases with decreasing  $f$ . However, for  $f = 1$ , here we obtain  $R_g = 4.8$  which is clearly smaller than the value  $R_g = 6.4$  obtained in run A (see Fig. 6). This proves that for  $l_b = 4$  the chain conformation stays as a globule, since we already found that for the same chain length and with  $l_b = 10$  the chain conformation was compact and two-dimensional. In the case under consideration ( $f = 1$ ,  $l_b = 4$ ), the value of  $R_g = 4.8$  is almost identical to the one obtained in the bulk where  $R_g = 4.4$  (see Table II).

Upon reducing  $f$  (run F and G), the chain is much more expanded and it is found that  $R_g = 9.4$ . Taking into account the fact the chain is still adsorbed for both systems (run F and G) as was found in the analysis of the adsorption profile (see Fig. 11), one deduces that the spreading of the monomers is very important as soon as  $f < 1$ . A comparison with the strong Coulomb coupling shows that values of  $R_g$  for  $l_b = 4$  are systematically larger than those of  $R_g$  with  $l_b = 10$  (see Fig. 6 and Table II), indicating again that the chain fluctuates more in the outward macroion radial direction at weaker Coulomb coupling.

TABLE IV : Polyelectrolyte overcharge  $\rho_{PE}$  values as a function of  $f$  (runs E - G).

Run	$1=f$	$\rho_{PE}$
E	1	1.043 0.002
F	2	1.089 0.003
G	3	1.065 0.006

#### D . Polyelectrolyte overcharging

In order to check if the local polyelectrolyte overcharge is responsible for the expansion of the chain upon reducing  $f$  as was demonstrated in the strong Coulomb coupling for  $b_b = 10$  in Sec. IIIB 5, we again consider the overcharging ratio  $\rho_{PE}$  defined by Eq. (13) with the same condensation distance  $\kappa_c = 1.2$  as was done for  $b_b = 10$  in Sec. IIIB 5.

Numerical values of  $\rho_{PE}$  are can be found in Table IV. It clearly shows that polyelectrolyte overcharge is negligible (i. e.,  $\rho_{PE} \approx 1$ ) for the present Coulomb coupling regime whatever the value of  $f$ . Consequently one can not explain the expansion of the chain with increasing  $1=f$  with a polyelectrolyte overcharge mechanism. We will give clear and qualitative arguments in Sec. VI that account for these conformations.

#### V . W E A K C O U L O M B C O U P L I N G

This part is devoted to aqueous solutions where the Bjerrum length is  $b_b = 2 = 7.14$  Å corresponding to the dielectric constant  $\epsilon_r = 80$  of water. Such systems will be referred to as the weak Coulomb coupling regime. We have considered a set of three runs H - J (see Table II) identical to the previous ones but with a shorter Bjerrum length  $b_b = 2$ . Again it is helpful to start with the description of the observed complex microstructures.

##### A . C o m p l e x m i c r o s t r u c t u r e

Typical equilibrium macroion-polyelectrolyte complex structures can be found in Fig. 12. For all investigated cases (runs H - J), one finds that the polymer never adopts a "two-dimensional" conformation. A comparison of the bulk value of  $R_g$  and the  $R_g$  of the chain in the complexed situation (compare Table II) reveals that the chain conformation is only weakly affected by the macroion. For the fully charged polymer ( $f = 1$ , run H), the conformation is again rather compact but without exhibiting a strong monomer-counterion ordering (within the polymeric aggregate) as it was the case for higher Coulomb coupling regimes [compare Fig. 12 (a) with Fig. 10 (a) and Fig. 4 (a)]. However we do have an effective macroion-polyelectrolyte attraction, and the dense monomer-counterion aggregate is adsorbed onto the colloidal surface.

For  $f = 1/2$  (run I), the chain conformation is more expanded than for  $f = 1$  [compare Fig. 12 (b) with Fig. 12 (a)]. Nevertheless we do have polymer adsorption with the formation of chain loops. Therefore even for couplings which are typical of aqueous systems, our simulations show that like-charge complexation can occur for  $f = 1$  and  $f = 1/2$  with divalent ions ( $Z_m = Z_c = 2$ ).

For even lower linear charge density ( $f = 1/3$ , run J), Fig. 12 (c) shows polymer desorption from  $f = 1/2$  to  $f = 1/3$ . In the same time there is a certain "counterion release" for  $f = 1/3$ , meaning that not all counterions are in the vicinity of the highly charged objects (macroion and polyelectrolyte). We carefully checked that, with periodic boundary conditions, the same features qualitatively appear, namely chain desorption from  $f = 1/2$  to  $f = 1/3$ .

##### B . A d s o r p t i o n p r o f i l e

Integrated distribution  $P(r)$ , radial distribution  $n(r)$  and fluid net charge  $Q(r)$  profiles are depicted in Figs. (a-c) respectively. The ion fraction  $P(r)$  profiles show that for  $f = 1$  (run H) and  $f = 1/2$  (run I) almost all atoms lie within a distance  $a < r < 20$  [i. e.  $P(r = 20) \approx 1$ ], corresponding to roughly one macroion diameter away from the colloidal surface [see Fig. 13 (a)]. This is in contrast to what was previously found (with  $f = 1$  and  $f = 1/2$ ) at stronger Coulomb coupling regimes where almost all ions lie within a distance of a few monomer sizes from the macroion surface [compare Fig. 13 (a) with Fig. 5 (a) and Fig. 11 (a)]. For  $f = 1/3$  (run J) only a very small fraction of monomers [ $P_m(r = 10) < 5\%$ ] lie in the vicinity of the macroion surface. In this latter situation, the counterion  $P_c(r)$  profile indicates that a larger fraction of counterions float in the solution. Because the  $R_g$  of the chain is

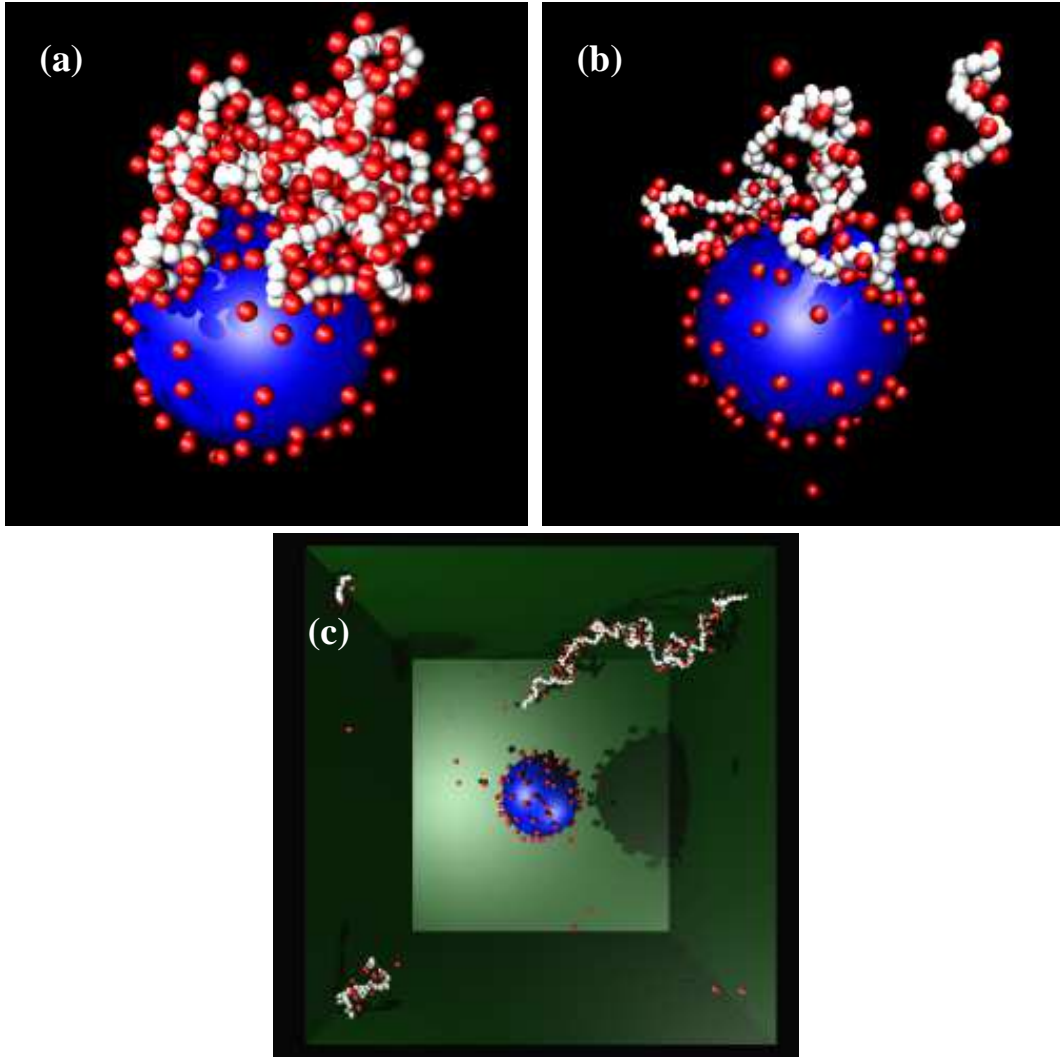


FIG. 12: Typical equilibrium configurations of the colloid-polyelectrolyte complex in weak Coulomb coupling ( $l_b = 2$ ) for (a) run H ( $f = 1$ ), (b) run I ( $f = 1/2$ ) and (c) run J ( $f = 1/3$ ). Monomers are in white and counterions in red. Snapshot (c) was obtained with periodic boundary conditions.

very large and some chain monomers might be interacting with the cell boundary we performed for this situation a simulation where we employed periodic boundary condition, and where the interactions were computed using the P3M algorithm<sup>34</sup>. With this run we found no chain monomers in the vicinity of the colloid surface, hence unambiguously found monomer desorption from the colloidal surface.

Concerning the intra-chain monomer ordering for  $f = 1$ , Fig. 13 (b) shows that, although the chain conformation is relatively dense, there is only one main peak in the monomer  $n_m(r)$  profile (the second peak is marginal). This proves that there is no strong intra-chain monomer ordering (in the normal direction to the macroion sphere) in this weak Coulomb coupling in contrast with our observations at  $l_b = 4$  [compare with Fig. 11 (b)]. Nevertheless a second counterion layer (third monomer layer) is build. The height  $h_m$  of the monomer peak is identical (within the statistical uncertainty) for  $f = 1$  and  $f = 1/2$  and corresponds to  $h_m = 0.038 \sigma^{-1}$ , whereas for  $f = 1/3$  we have  $h_m = 0.01 \sigma^{-1}$ .

As far as the net fluid charge  $Q(r)$  is concerned, Fig. 13 (c) shows that for  $f = 1$  a weak charge oscillation appears with a marginal macroion overcharge compensation of 3%. For  $f = 1/2$ , the same marginal macroion overcharging occurs but without exhibiting charge oscillation. Finally, for  $f = 1/3$  no overcharging appears and the net charge increases monotonically.

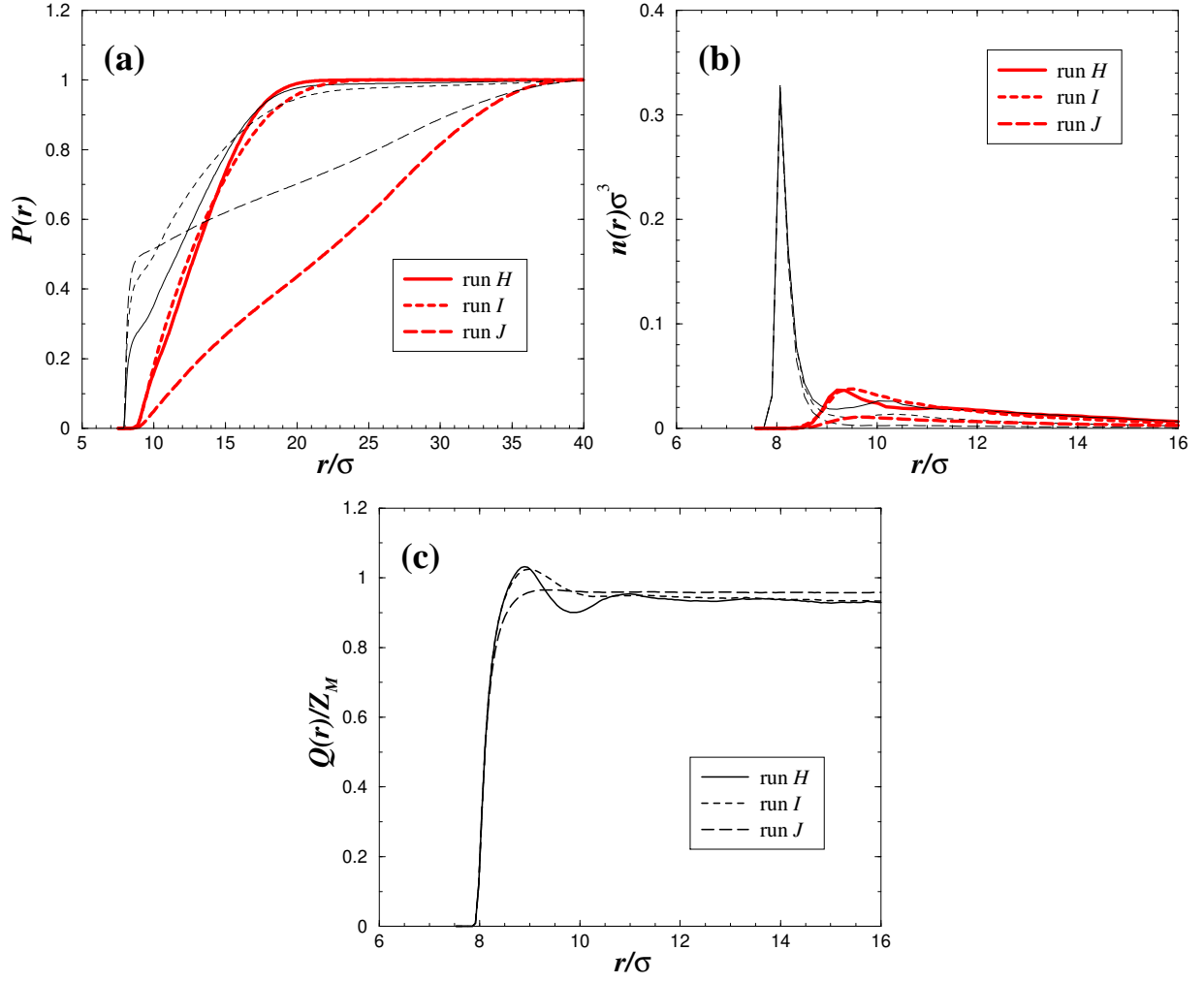


FIG. 13: Ion adsorption profiles (runs H – J) as a function of the distance  $r$  from the macroion center. (a) Fraction  $P(r)$  and (b) radial density  $n(r)$  of counterions (thin lines) and monomers (thick lines) adsorbed on the spherical macroion. (c) Reduced net fluid charge  $Q(r) = Z_M$ .

#### C. Polyelectrolyte chain radius of gyration

In Fig. 6 (for  $l_b = 2$ ) the chain radius of gyration  $R_g$  as function of  $f$  is plotted. It is found that  $R_g$  increases almost linearly with  $l = f$ . This result fits well with the scaling theory in this regime from Ref.<sup>35</sup> where it is found that the chain extension shrinks proportionally with  $l_b$ , and we can assume for our purposes  $f \propto l_b$ . Because the electrostatic interactions are weaker in the present case ( $l_b = 2$ ), the ion pair (monomer – condensed counterion) attractions are weaker which results in a higher  $R_g$  value (at fixed  $f$ ) than in the strong Coulomb coupling regime.

#### D. Monovalent case, $f = 1$

Our last result concerns the monovalent case ( $Z_m = Z_c = 1$  and  $f = 1$ ) corresponding to run K (see Table II). In this situation we have a strong macroion-polyelectrolyte repulsion, and one can not get like-charge complexation.



## VI. CONCLUDING REMARKS

We have carried out MD simulations to study the complexation of a charged colloid with a charged polyelectrolyte of the same charge for various Coulomb couplings  $\ell_b$  and varying charge fraction  $f$ .

For  $\ell_b = 10$  we gave a reasoning for the observed conformation in terms of overcharging of the single chain. However this argument only worked for the largest coupling parameter.

A complementary view of the observed conformations is to regard both macroions as being neutralized by their counterions. The isolated chain would then collapse into a globule, and the colloid would be regularly covered by its counterions. By changing the Bjerrum length  $\ell_b$  we change the correlations between the charges which lead in a first approximation to attractions of dipolar origin, and the attraction is roughly proportional to  $\ell_b$ . On the other hand, by varying  $f$  we change the number of counterions of the chain, hence the number of available dipoles.

For  $f = 1$  we can regard the colloidal particle as exerting only a perturbation of the chain complex (which has a higher density of dipoles). For largest  $\ell_b$  the strong attraction results in a flat disk, for weaker  $\ell_b$  the disk swells back into the bulk structure, the globule. For smaller  $f$  the number of counterions of the polyelectrolyte and the colloid become comparable in number, and both macroions can equally compete for the counterions leading to a greater freedom of both macroions to "move" in their common counterion cloud. For the largest value of  $\ell_b$  we have again the strongest dipolar attractions leading to a purely 2D conformation, where the chain is wrapped around the colloid. For smaller values of  $\ell_b$  the conformations become more and more 3D-like, but are still wrapping around the colloid. Of special interest is here the fact that even for a coupling strength which is typically for an aqueous solvent ( $\ell_b = 7.1$  Å) we find that like-charge complexation still occurs provided the linear charge density is sufficiently large. However the adsorption of the polymer chain onto the colloid is weaker than in the larger Coulomb coupling regimes. For  $f = 1/2$ , we observe formation of large loops.

For  $\ell_b = 2$  and  $f = 1/3$  we find no complex, but end with two single macroions together with their counterion cloud which interact mainly with their bare charge, i.e. repulsive.

Our parameters concerning aqueous solutions should be experimentally accessible, typically for small highly charged colloids (micelles and relatively short polyelectrolyte chains).

## Acknowledgments

This work is supported by Laboratoires Europeens Associés (LEA).

---

Electronic address: messina@mpip-mainz.mpg.de

<sup>7</sup> Electronic address: holm@mpip-mainz.mpg.de

<sup>2</sup> Electronic address: k.kremer@mpip-mainz.mpg.de

<sup>1</sup> K.E. van Holde, *Chromatin* (Springer, New York, 1989).

<sup>2</sup> D.W. M. C. Quigg, J.I. Kaplan, and P.L. Dublin, *J. Phys. Chem.* **96**, 1973 (1992).

<sup>3</sup> M. G. Runstein, *Nature* **389**, 349 (1997).

<sup>4</sup> F. Caruso, R.A. Caruso, and H. Mohwald, *Science* **282**, 1111 (1998).

<sup>5</sup> F. von Goeler and M. Muthukumar, *J. Chem. Phys.* **100**, 7796 (1994).

<sup>6</sup> N.L. Marky and G.S. Manning, *J. Mol. Biol.* **255**, 50 (1995).

<sup>7</sup> E. Gurovitch and P. Sens, *Phys. Rev. Lett.* **82**, 339 (1999).

<sup>8</sup> E.M. Matescu, C. Jeppesen, and P. Pincus, *Europhys. Lett.* **46**, 493 (1999).

<sup>9</sup> S.Y. Park, R.F. Bruinsma, and W.M. Gelbart, *Europhys. Lett.* **46**, 454 (1999).

<sup>10</sup> R.R. Netz and J.F. Joanny, *Macromolecules* **32**, 9026 (1999).

<sup>11</sup> H. Schiessel, J. Rudnick, R. Bruinsma, and W.M. Gelbart, *Europhys. Lett.* **51**, 237 (2000).

<sup>12</sup> K.-K. Kunze and R.R. Netz, *Phys. Rev. Lett.* **85**, 4389 (2000).

<sup>13</sup> T.T. Nguyen and B.I. Shklovskii, *Physica A* **293**, 324 (2001).

<sup>14</sup> T. Wallin and P. Linse, *Langmuir* **12**, 305 (1996).

<sup>15</sup> T. Wallin and P. Linse, *J. Phys. Chem.* **100**, 17873 (1996).

<sup>16</sup> T. Wallin and P. Linse, *J. Phys. Chem. B* **101**, 5506 (1997).

<sup>17</sup> C.Y. Kong and M. Muthukumar, *J. Chem. Phys.* **109**, 1522 (1998).

<sup>18</sup> M. Jonsson and P. Linse, *J. Chem. Phys.* **115**, 3406 (2001).

<sup>19</sup> R. Messina, C. Holm, and K. Kremer, to appear in *Phys. Rev. E*.

<sup>20</sup> K. Kremer and G. Grest, *J. Chem. Phys.* **92**, 5057 (1990).

<sup>21</sup> I. Rouzina and V.A. Bloomfield, *J. Chem. Phys.* **100**, 9977 (1996).

<sup>22</sup> R. Messina, C. Holm, and K. Kremer, *Phys. Rev. Lett.* **85**, 872 (2000).

- <sup>23</sup> R. Messina, C. Holm, and K. Kremer, Phys. Rev. E 64, 021405 (2001).
- <sup>24</sup> R. Messina, C. Holm, and K. Kremer, Europhys. Lett. 51, 461 (2000).
- <sup>25</sup> R. Messina, C. Holm, and K. Kremer, Eur. Phys. J. E 4, 363 (2001).
- <sup>26</sup> B. Shklovskii, Phys. Rev. E 60, 5802 (1999).
- <sup>27</sup> M. J. Stevens and K. Kremer, Phys. Rev. Lett. 71, 2228 (1993).
- <sup>28</sup> M. J. Stevens and K. Kremer, J. Chem. Phys. 103, 1669 (1995).
- <sup>29</sup> R. G. Winkler, M. Gold, and P. Reineker, Phys. Rev. Lett. 80, 3731 (1997).
- <sup>30</sup> R. Golestanian, M. Kardar, and T. B. Liverpool, Phys. Rev. Lett. 82, 4456 (1999).
- <sup>31</sup> N. V. Brilliantov, D. V. Kuznetsov, and R. Klein, Phys. Rev. Lett. 81, 1433 (1998).
- <sup>32</sup> This argument assumes that the ions (charged monomers + condensed counterions) distribution along the chain is uniform. This should be relatively well satisfied since the bare charged monomers are already uniformly distributed.
- <sup>33</sup> This reasoning holds in the strong Coulomb coupling regime where the polymer structure is essentially dictated by the charged (effective) monomers.
- <sup>34</sup> M. Deserno and C. Holm, J. Chem. Phys. 109, 7678 (1998).
- <sup>35</sup> H. Schiessel and P. Pincus, Macromolecules 31, 7953 (1998).